สัญญาเลขที่ R2559C052

รายงานวิจัยฉบับสมบูรณ์

การประดิษฐ์เซรามิกใหม่ $(Ba_{0.97}Ca_{0.03})(Zr_{0.94}Sn_{0.06})O_3$ ด้วยเทคนิคการเผาไหม้

Fabrication of New $(Ba_{0.97}Ca_{0.03})(Zr_{0.94}Sn_{0.06})O_3$ Ceramics by the Combustion Technique

ผศ.ดร.ธีระชัย บงการณ์
ภาควิชาฟิสิกส์ คณะวิทยาศาสตร์ มหาวิทยาลัยนเรศวร

สนับสนุนโดยกองทุนวิจัยมหาวิทยาลัยนเรศวร

หัวข้อวิจัย การประดิษฐ์เซรามิกใหม่ $(Ba_{0.97}Ca_{0.03})(Zr_{0.94}Sn_{0.06})O_3$ ด้วยเทคนิคการเผาไหม้

นักวิจัย ผศ.ดร.ธีระชัย บงการณ์

บทคัดย่อ

ศึกษาสมบัติของเซรามิก $(Ba_{0.97}Ca_{0.03})(Zr_{0.94}Sn_{0.06})O_3$ (BCZS) ด้วยวิธีการเผาไหม้ โดยศึกษาผลของอุณหภูมิที่มีต่อการก่อเกิดเฟส โครงสร้างจุลภาค และสมบัติทางไฟฟ้าของเซรามิก BCZS เซรามิก BCZS เตรียมด้วยวิธีการเผาไหม้ โดยใช้ไกลซีนเป็นเชื้อเพลิง ภายใต้เงื่อนไขการเผาแคลไซน์ที่อุณหภูมิ 1000-1200 °C เป็นเวลา 2 ชั่วโมง และซินเตอร์ที่อุณหภูมิ 1500-1675 °C เป็นเวลา 2 ชั่วโมง พบเฟสเพอรอฟสไกต์บริสุทธ์ ที่อุณหภูมิแคลไซน์สูงกว่า 1150 °C และพบเฟสเพอรอฟสไกต์บริสุทธิ์ทุกตัวอย่างเซรามิก เมื่อเพิ่มอุณหภูมิในการเผาค่าเฉลี่ยขนาดอนุภาคและขนาดเกรนเพิ่มขึ้นจาก 73 ถึง 103 นาโนเมตร และจาก 0.51 ถึง 1.61 ไมโครเมตร ตามลำดับ จากการเผาแคลไซน์ที่อุณหภูมิต่ำ อนุภาคมีลักษณะเป็นทรงกลมเกาะกลุ่มอยู่กันอย่างหนาแน่น เมื่อเพิ่มอุณหภูมิสูงขึ้นอนุภาคทรงกลมจับตัวกันแบบหลวม ๆ ไม่คับแน่น ค่าความหนาแน่นสูงสุดถูกพบที่ตัวอย่างเผาซินเตอร์ที่อุณหภูมิ 1650 °C ซึ่งแสดงค่าคงที่ไดอิเล็กทริกและค่าการสูญเสียไดอิเล็ก ทริก ความถี่ 100 kHz ณ อุณหภูมิห้อง เท่ากับ 44 และ 0.01 ตามลำดับ

Research Topic: Fabrication of New $(Ba_{0.97}Ca_{0.03})(Zr_{0.94}Sn_{0.06})O_3$ Ceramics by the Combustion Technique

Researcher: Assist.Prof.Dr.Theerachai Bongkarn

ABSTRACT

In this study, properties of $(Ba_{0.97}Ca_{0.03})(Zr_{0.94}Sn_{0.06})O_3$ ceramics (abbreviated as BCZS) was prepared by the solid state combustion technique. The experimental processes are focused on the effects of firing temperatures on phase formation, microstructure and electrical properties of BCZS ceramics. BCZS ceramics were synthesized by the combustion technique using glycine as fuel. The powders and ceramics were calcined from 1,000 to 1,200 °C for 2 h and sintered from 1,500 to 1,675 °C for 2 h. A pure perovskite phase was found in the powder calcined at higher than 1,150 °C and the purity phase of the ceramics was detected in all samples. The average particle size and grain size increased approximately from 73 to 103 nm and from 0.51-1.61 μm, respectively when firing temperatures increased. The calcined powders exhibited tight agglomerates at low calcination temperatures and they changed to loosely bound agglomerates at higher calcination temperatures. The densest ceramics were discovered in the samples sintered at 1,650 °C. The dielectric constant (ε_r) and loss factor (tan δ) values measured at 100 kHz of this sample were found to be 44 and 0.01, respectively at room temperature.

CHAPTER I

INTRODUCTION

Rationale for the study and statement of the problem

In the present, electronics are very important in our daily life. Advances in these are transforming our world at an unbelievable pace. Piezoelectric materials are the most important and widely used materials for transducers, transformers, sensor, actuator, buzzers and other electronic devices. The most widely used piezoelectric materials are lead zirconate titanate (PZT) ceramics due to their excellent electrical properties [1]. However, these ceramics are toxic in the environment and damage to human health. The best way of prevention is to avoid the contact with leaded materials [2]. Therefore, it is necessary in the search for lead-free piezoelectric materials to replace PZT ceramics.

Barium zirconate ($BaZrO_3$) is one of the perovskite material with an ideal cubic structure and has a high melting point of about 2,600 °C. Barium zirconate is a good candidate for many applications such as dielectrics for microwave components [3], crucible material [4] and for use in the electric industry as insulators [5]. The preparation of $BaZrO_3$ is difficult to sinter and the densification of the ceramics is a challenge. The preparation of $BaZrO_3$ is difficult to sinter and the densification of the ceramics is a challenge. A.M. Azad, et al. [6] synthesized pure cubic perovskite $BaZrO_3$ powder using the solid reaction method and obtained ~90% of theoretical density employing heat treatment at 1,600 °C for 6 and then increasing the heat to 1,700 °C without any dwell time. A. Sin, et al. [7] reported a value of 95% of theoretical density of $BaZrO_3$ ceramics. They synthesized nano $BaZrO_3$ powders by the polyacrylamide method. The sintered ceramics were obtained using a heat treatment of 1,500 °C for 10 h. Nano $BaZrO_3$, powders (25-30 nm) and low firing temperatures (calcined at 800 °C, sintered at 1,000 °C) were obtained using microemulsion route [8]. B. Guillaume, et al. [9] successfully prepared 99% of theoretical density of $BaZrO_3$ ceramics by control the calcined powder size distribution. The mean particles size of 600 nm was sintered at 1,650 °C for 2 h. A.M.

Azad and S. Subramaniam [10] attempted to improve the density and dielectric properties by adding 5 mol% Sn in $BaZrO_3$. The attempt to improve the density was not successful but with a dielectric loss of the $Ba(Zr_{0.95}Sn_{0.05})$ ceramics exhibited a very small value and were stable in a wide frequency range (1-10^6 Hz). Recently, W. Li, et al. [11] succeeded in increasing the density (99% of theoretical density) of $Ba(Ti_{0.94}Sn_{0.06})O_3$ ceramics by the addition of 3 mol% Ca at the A site. The substitution of Ca promoted the microstructure of $Ba(Ti_{0.94}Sn_{0.06})O_3$, which presented a clear grain boundary and a uniformly distributed grain size. It also resulted in increased density and better electrical properties. $(Ba_{0.97}Ca_{0.03})(Ti_{0.94}Sn_{0.06})O_3$ which exhibited excellent piezoelectric properties (d_{33}=440 pC/N, kp=45%), a high dielectric constant (ε_r= 6,900) and a low dielectric loss (tan δ=0.015). The B site of $Ba(Zr_{0.95}Sn_{0.05})O_3$ and $Ba(Ti_{0.94}Sn_{0.06})O_3$ is mainly possessed by different Zr and Ti, but the ionic radius of Zr^{4+} (0.072nm) is close to the ionic radius of Ti^{4+}(0.061nm). Therefore, the idea of the addition of 3 mol% Ca and 6 mol% Sn into the A and B site of $BaZrO_3$ increasing the density, decreasing the dielectric loss and stabilizing the dielectric constant are interesting and challenging.

Recently, there has been interest shown in the solid state combustion technique is modified from the solid-state reaction technique and has become an attractive technique to prepare high quality ferroelectric ceramics. It helps to decrease the temperature in the preparation and result in an ultrafine particle size. The energy released from the decomposition reaction of fuel speeds up the chemical reaction of raw materials. Moreover, the liquid phase caused from the melting of fuel creates an easier chemical reaction of raw materials. The combustion reaction technique also has interesting characteristics such as its simplicity, this relatively low cost, the fact that it usually results in products with the desired structure, composition, densities and good electric properties [12, 13, 14, 15].

Furthermore, a detailed study of BCZS ceramics fabrication using the solid state combustion technique have not been reported in the literature. Therefore, The main objectives of this study are to obtain the pure perovskite phase $(Ba_{0.97}Ca_{0.03})(Zr_{0.94}Sn_{0.06})O_3$ (BCZS) by the solid state combustion technique to decrease complication and reduce the firing temperatures were studied. The effects of

CHAPTER II

THEORY AND LITERATURE

This chapter contains details on the brief description of necessary concepts of the perovskite ferroelectrics. In addition, the relevant literatures on processing and characteristics of both powders and ceramics are reviewed with attention paid on their properties.

Perovskite Structure

Since the ferroelectric properties of barium titanate were reported by Von Hippel in 1945, ABO_3 compound with the perovskite structure have been studied extensively. These studies have resulted in the discovery of many new ferroelectric and piezoelectric materials. Most of the literatures on perovskite-type compounds have concentrated on these properties.

Perovskite structure is a crystal structure of a mineral perovskite calcium titanate ($CaTiO_3$) which was discovered by Count Lev Aleksevich von Perovski [16]. This structure is adopted by many oxides that the general chemical formula of ABO_3. The general crystal structure is a primitive cube which the A represents a cation with larger ionic radius in the corner, B represents a cation with a smaller ionic radius in the middle of the cube and O is oxygen in the centre of the face edges. Figure 1 shows a cubic perovskite structure unit cell (a) and three-dimensional network of BO_6 octahedra (b). The sites are occupied by Ba^{2+}, Pb^{2+}, K^+ or Na^+ ions, and B sites by Ti^{4+}, Zr^{4+}, Nb^{5+} or Ta^{5+} ions. Some examples of perovskite-type ceramic compounds are lead titanate ($PbTiO_3$), barium titanate ($BaTiO_3$), bismuth sodium titanate ($Bi_xNa_{1-x}TiO_3$), potassium niobate ($KNbO_3$), etc. The perovskite structure can tolerate a wide range of compositional variation. Thus, its properties are differed behavior [1, 17, 18].

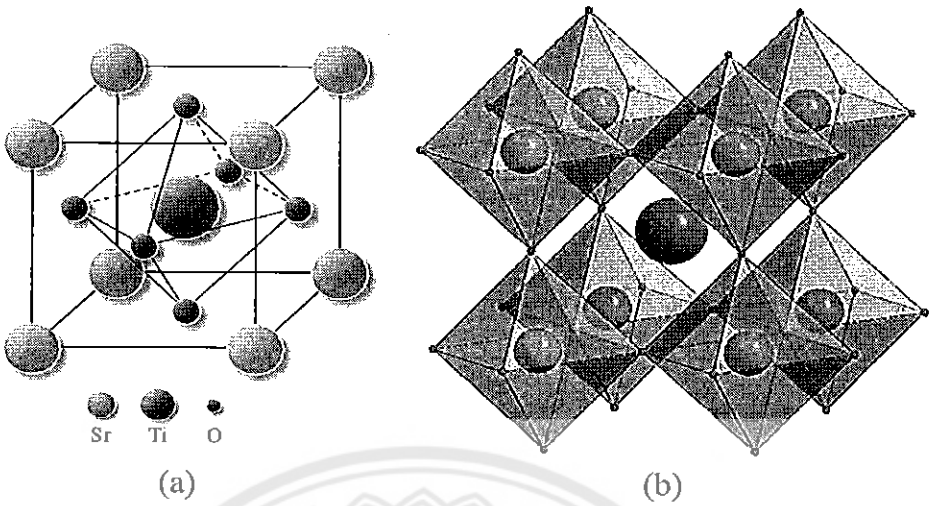

Figure 1 (a) A cubic $SrTiO_3$perovskite-type unit cell and (b) three-dimensional network of BO_6 octahedra [16]

Piezoelectricity

Piezoelectricity was discovered in 1880 by Jacques and Pierre Curie during their systematic study of the effect of pressure on the generation of a electrical charge by crystals such as quartz, zincblend, and tourmaline [18]. The name "piezo" is derived from the Greek, meaning "to press", hence piezoelectricity is the generation of electricity as a result of mechanical pressure. Many piezoelectric materials are not ferroelectric but all ferroelectrics are piezoelectric. Two effects are operative in piezoelectricity. The direct effect is identified with the phenomenon whereby an electrical charge (polarization) is generated from mechanical stress, whereas the converse effect is associated with the mechanical movement generated by the application of an electrical field. Both of these effects are illustrated in Figure 2.

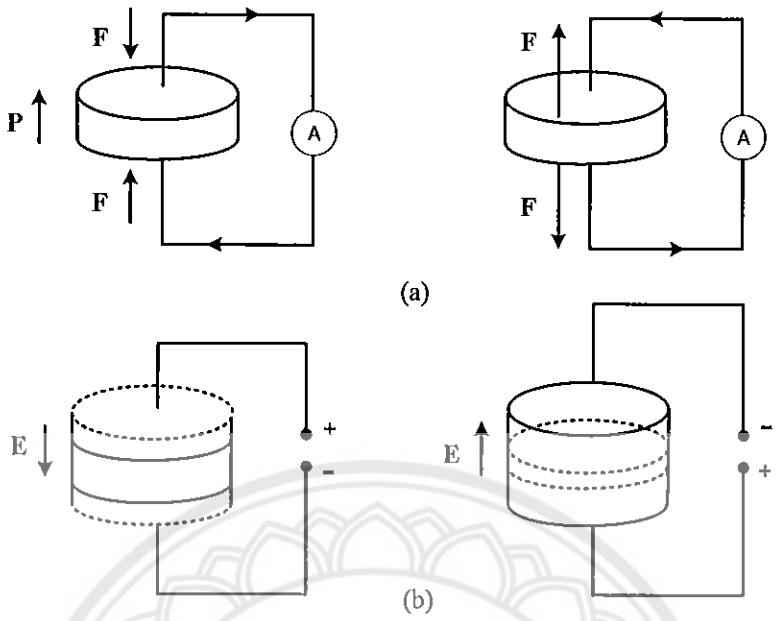

Figure 2 Piezoelectric effects in ferroelectric ceramics
(a) direct effect (b) converse effect [18]

The basic equations that describe these two effects in regard to electric and elastic properties are

$$D = dT + \varepsilon^T E \quad (1)$$

$$S = s^E T + dE \quad (2)$$

Where D is the dielectric displacement (consider it equal to polarization), T the stress, E the electric field, S the strain, d a piezoelectric coefficient, s the material compliance (inverse of modulus of elasticity), and ε the dielectric constant (permittivity). The subscripts indicate a quantity held constant: in the case of ε^T, the stress is held constant, which means that the piezoelectric element is mechanically unconstrained, and, in the case of s^E, the electric field is held constant, which means the electrodes on the element are shorted together.

Ferroelectrics

Ferroelectricity is a phenomenon which was discovered by Valasek in 1921 [19]. It has become customary to call ferroelectricity the phenomenon exhibited by these crystals and ferroelectric the crystal themselves. This is due to a formal similarity of the ferroelectric phenomenon with that of ferromagnetism. The similarity is mainly phenomenological. As ferromagnetic materials exhibit a spontaneous magnetization and hysteresis effects in the relationship between magnetization and magnetic field, ferroelectric crystals show a spontaneous electric polarization and hysteresis effects in the relation between the dielectric displacement and the electric field. This behavior is mostly observed in certain temperature regions below by transition temperature (Curie temperature) where those crystals above are this transition temperature are no longer ferroelectric.

The crystal symmetries of the paraelectric and ferroelectric phase are an important factor in displaying the ferroelectric behavior of the materials. The lattice structure described by the Bravais unit cell of the crystal governs the crystal symmetry. Though there are thousands of crystals in nature, they all can be grouped together into 230 microscopic symmetry types or space groups based on symmetry elements. It can be shown by the inspection of the 230 space groups that there are just 32 point groups. As shown in Figure 3, the 32 point groups can be further classified into (a) crystal having a center of symmetry and (b) crystals which do not possess a center of symmetry (noncentrosymmetric). There are 21 classes of noncentrosymmetric, a necessary condition for piezoelectricity to exist, and only 20 are piezoelectric. Among these 20 point groups, only 10 can display a spontaneous polarization, which is designated as pyroelectric. A subgroup of the spontaneous polarized pyroelectric is a category of materials known as ferroelectrics. Ferroelectrics are a special class of materials in which a permanent electric dipole can be reoriented between equilibrium states by the external electric field. Continuing Valasek's analogy between ferroelectric and ferromagnetic, the dependence of the polarization on an applied electric field can be seen by polarization versus electric field i.e. (P-E) hysteresis loop as shown in Figure 4. The hysteresis loop is typically observed using the simple circuit described by Sawyer-Tower [30]. One parameters obtained from the hysteresis loop measurement, the remnant polarization (P_r) is the crystal spontaneous

polarizes along one of the allowed direction without applied electric field. The field required to reverse the polarization is known as the coercive field (E_c).

Normal ferroelectric materials have a sharp phase transition which occurs at a specific temperature called the Curie temperature, T_c. The T_c is the temperature which the crystal structure transforms from the paraelectric state into the ferroelectric state and vice versa [1, 21, 22]. In the paraelectric state, the dielectric permittivity obeys the Curie-Weiss law.

$$\varepsilon_r = \frac{C}{T - T_0} \tag{3}$$

Where C is the Curie-Weiss constant, T is the temperature and T_0 is the Curie-Weiss temperature. The Curie temperature (T_c) and the Curie-Weiss temperature (T_0) should not be confused. The Curie temperature is the actual transformation temperature, but the Curie-Weiss temperature is found by extrapolating the plot of the Curie-Weiss law, as shown in Figure 5. The Curie temperature and Curie-Weiss temperature typically differ by only a small amount that depends on the type of phase formation the material undergoes. The Curie-Weiss temperature can be as much as ten degrees lower than the Curie temperature for first-order phase transformations and the two can be nearly equal for second-order phase transformations (first order phase transformations are those in which the first derivative of the free energy, with respect to temperature, is discontinuous; second order phase transitions are those in which the second derivative is discontinuous).

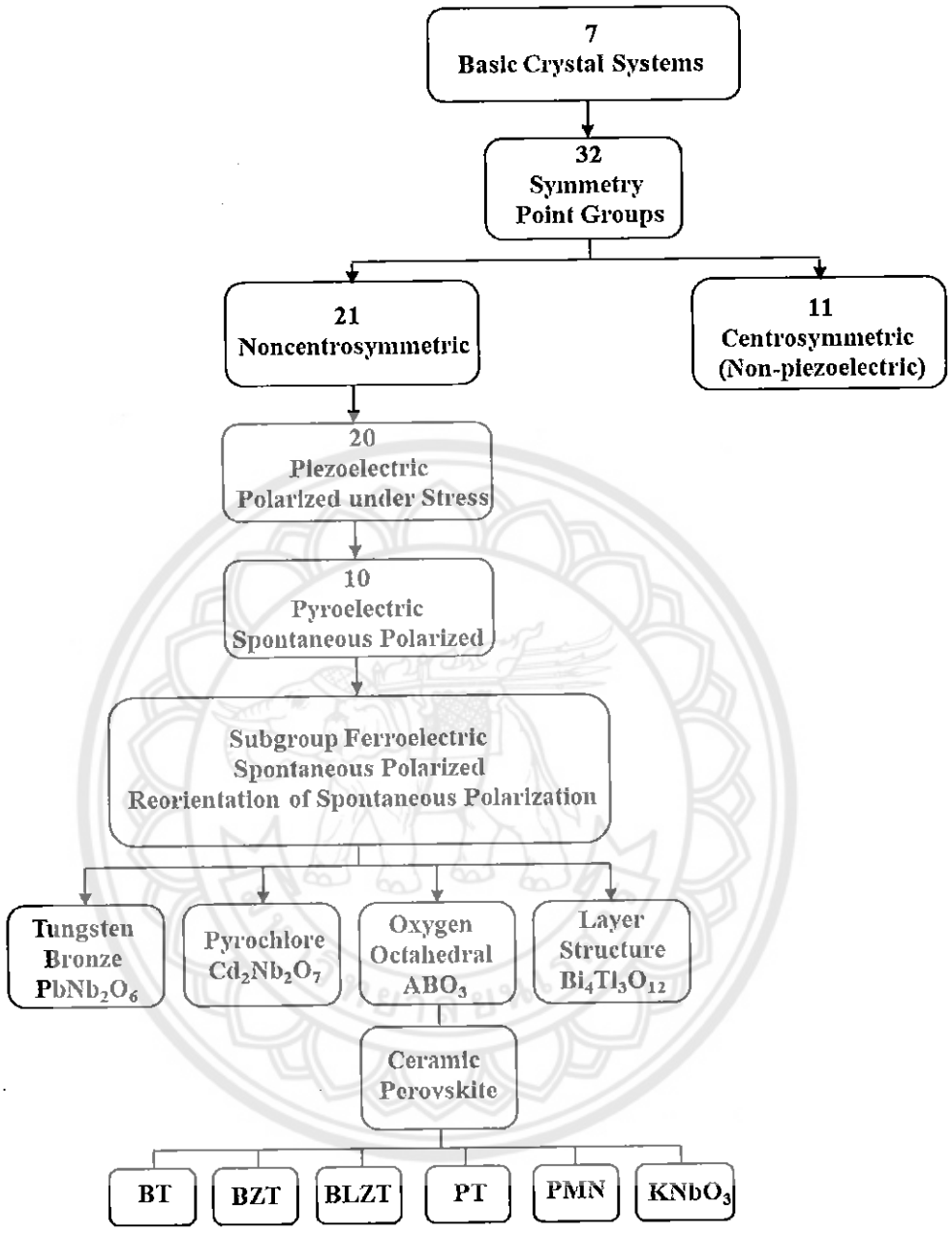

Figure 3 Interrelationship of piezoelectric and subgroups on the basis of symmetry [17]

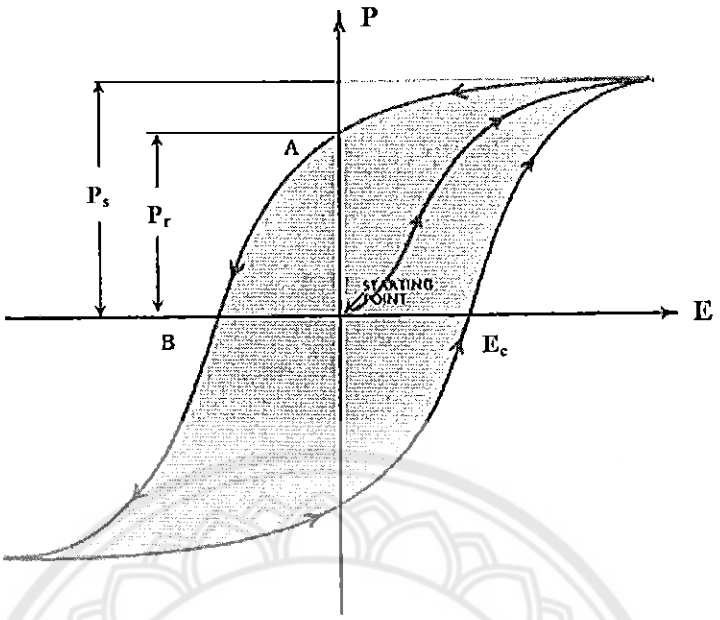

Figure 4 A ferroelectric hysteresis loop [20]

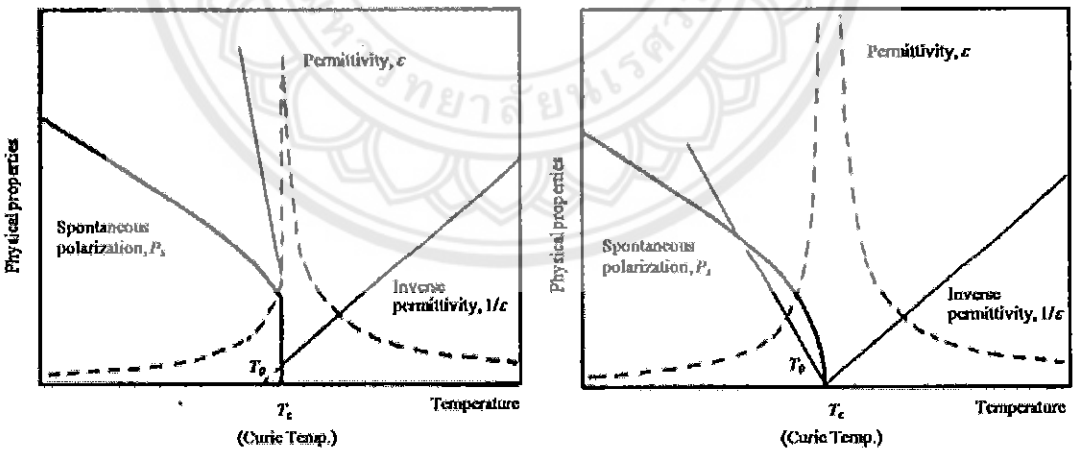

Figure 5 Phase transition in a ferroelectric (a) first order and (b) second order [21]

Antiferroelectric

An antiferroelectric crystal is defined as a crystal whose structure can be considered as being composed of two sublattices polarized spontaneously in antiparallel directions and in which a ferroelectric phase can be induced by applying an electric field. Experimentally, the reversal of the spontaneous polarization in ferroelectrics is observed as a single hysteresis loop, and the induced phase transition in antiferroelectrics as a double hysteresis loop (Figure 6), when a low-frequency ac field of a suitable strength is applied [23].

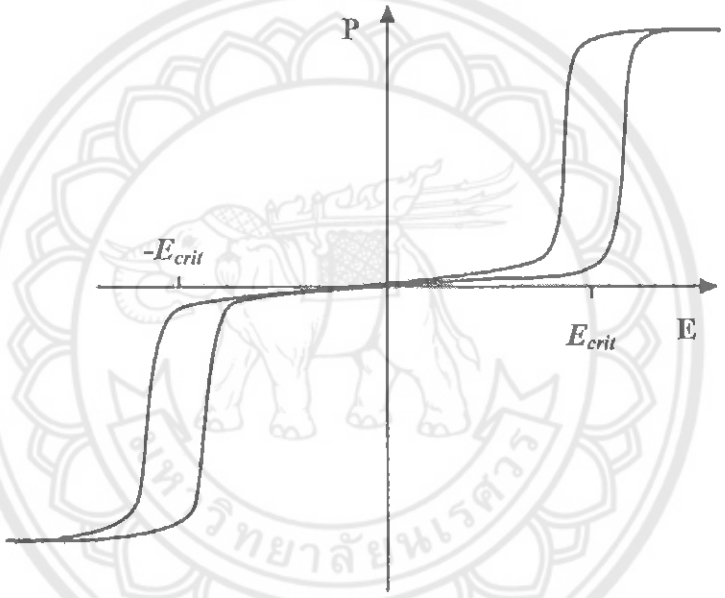

Figure 6 Antiferroelectric hysteresis loop [23]

Paraelectric

Paraelectricity is the ability of many materials (specifically ceramic crystals) to become polarized under an applied electric field. Unlike Ferroelectricity; this can happen even if there is no permanent electric dipole that exists in the material, and removal of the fields results in the polarization in the material returning to zero, as shown in Figure 7. The mechanisms which give rise to paraelectric behavior are the distortion of individual ions (displacement of the electron cloud from the nucleus) and the polarization of molecules or combinations of ions or defects. Paraelectricity occurs in crystal phases in which electric dipoles are unaligned (i.e. unordered

domains that are electrically charged) and thus have the potential to align in an external electric field and strengthen it. In comparison to the ferroelectric phase, the domains are unordered and the internal field is weak. The $LiNbO_3$ crystal is ferroelectric below 1430 K, and above this temperature it turns to paraelectric phase. Other perovskites similarly exhibit paraelectricity at high temperatures [24].

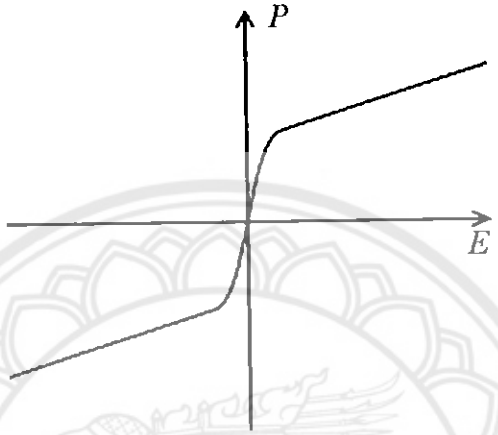

Figure 7 Paraelectric hysteresis loop [24]

Typical methods to synthesize ceramics

Solid-state reaction method

Solid-state reaction method is the most widely used method for the preparation of polycrystalline solids from a mixture of solid starting materials. This method involves chemical decomposition, where solid reactants are heated to produce a new solid and normally use simple oxides powders such as carbonates, hydroxides, nitrates, sulfates, acetates, oxalates, alkoxides and other metal salts for preparation. The solids do not react together at room temperature over normal time scales and it is necessary to heat them to much higher temperatures, often to 1000 to 1500 °C in order for the reaction to occur at an appreciable rate. An example of reaction between barium carbonate and titanium oxide at high temperature produce barium titanate by using solid-state reaction method.

$$BaCO_3(s) + TiO_2(s) \text{ -- (~1200 °C) -----> } BaTiO_3(s) + CO_2\,(g) \qquad (4)$$

Solid-state reactions generally have an advantage in terms of production cost. However, it is commonly understood that the conventional solid state method requires compulsory grinding of different oxide mixtures for long periods of time as well as sintering. In addition, the synthesized component distributions are not homogeneous and particle sizes are relatively large [25, 26].

Sol-gel processing

Sol-gel process is a method for producing solid materials from small moleculesin a solution (sols) agglomerate and under controlled conditions eventually link together to form a coherent network (gel). The method is used for many applications in synthesis of novel materials. The advantages of the sol-gel process in general are high purity, homogeneity and low temperature. For a lower temperature process, there is a reduced loss of volatile components are thus the process is more environmental friendly. In addition, some materials that cannot be made by conventional means because of thermal and thermodynamically instability can be made by this process. However, the disadvantages are also real. The starting materials can be fairly expensive [27, 28].

Co-precipitation method

Co-precipitation (CPT) is the carrying down by a precipitate of substances normally soluble under the conditions employed. This method proceeds in two stages. First stage, the impurity is trapped either on the surface or inside the growing particles. If the growing particles have a crystal structure, then the impurity will become localized at regions of the solid phase with a perfect structure. During rapid precipitation, the growing particles will trap non-equilibrium impurities, which are usually in homogeneously distributed through the volume of the solid phase. In the second stage, the concentration of defects within the precipitate decrease and the particles are flocculated. Impurities trapped during the first stage return either partially or completely to the medium. The concentration of impurities in the solid phase becomes equalized. The crystals acquire an equilibrium composition that depends only on the composition and temperature of medium [27, 28].

Combustion method

Combustion method is the method based on the principle that once a reaction is initiated under heating, an exothermic reaction occurs from the oxidation-reduction reaction between reaction materials and fuel. It has emerged as an important technique for the synthesis and processing of advanced ceramics, which involves a self-sustained reaction. The advantages of this technique include inexpensive raw materials, simple and fast preparation process, fine powders with high homogeneity and low firing temperature and shorter dwell time [29, 30, 31, 32]. The advantages of this method over other combustion methods are: firstly, being a solution process, it has control over the homogeneity and stoichiometry of the products; secondly, it is possible to incorporate desired impurity ions in oxide hosts and prepare industrially useful materials; thirdly, the process is simple and fast. Moreover, in fact, the reaction mechanism of this method is very complex due to there are several parameters influencing the reaction such as the type of fuel, fuel-oxidizer ratio, etc [33].

The fuel that used in combustion method was commonly an organic compound. Generally, a good fuel should reacted nonviolent, produce nontoxic gases, also acts as a chelating material for metal cations. It serve two purposes; first for the source of C and H which on combustion form CO_2 and H_2O and liberate heat and second for forming complexes with the metal ions facilitating homogeneous mixing of cations in solution. The nature of fuel and its amount are some of the important process parameter that influencing on the powder characteristics like a crystallite size, surface area nature of agglomeration, etc. The several fuels were used in the combustion method, e.g., urea, glycine, citric acid, alanine, carbohydrazide, poly acrylic acid, oxalic acid, acetyl acetone, metal acetate, hydrazine. Thus, the selection of an appropriate fuel is very important for the combustion system. Some properties of organic compounds used in combustion synthesis method are shown in Table 1. The commonly used fuels are; glycine, citric acid and urea. They were described as below;

1. Glycine

Glycine is one of the cheapest amino acids and is known to act as a complexing agent for a large amount of metallic ions. The glycine molecule has a carboxylic acid group located at one end of the chain and an amino group.

2. Citric acid

Citric acid is a weak organic acid that act as a convenient ligand which is inexpensive and is a more effective complexing agent for metal ions. The structure consists of three carboxyl groups and a hydroxyl group.

3. Urea

Urea is an attractive fuel for originating the formation of powders with crystallite sizes in the submicron/nanosized range and act as a complexing agent for metal ions because it contains two amino groups located at the extremes of its chemical structure.

Table 1 Some properties of organic compounds [34]

Properties	Organic component				
	Alanine	Glycine	Carbohydrazide	Urea	Citric acid
Structure formula	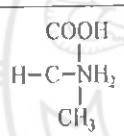	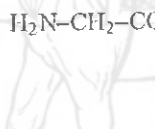	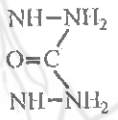	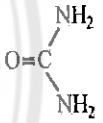	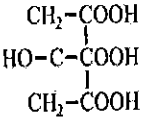
Molecular weight (g/mol)	80.1	90.1	75.1	60.1	192.1
Heat of combustion (kJ/g)	18.2	13.0	12.6	10.5	10.2
Decomposition temperature (°C)	314	262	153	135	175

The combustion method has been successfully used in the preparation of a large number of the ceramic oxide materials for a variety of applications which illustrated in Table 2. For example During the short span (> 15 years), many from the author's laboratory were becoming interested and attracted for producing fine grain size, crystalline and homogeneous ceramics at relatively low temperature and with reduced processing time. For example, Hwang, et al. [34] has investigated decomposition of the five fuels by acid or carbohydrazide. Some properties of five

fuels they select are shown in Table 1. The results of the thermal analysis show that there were different weight losses of organic fuels as presented in Figure 8. When using carbohydrazide as organic fuel, indicating that the chemical reaction took place very rapidly. But remaining weight is 22% of its original weight. While using glycine and alanine as organic fuels, the thermogravimetric of both demonstrated similar results. Their reactions are very fast and remaining weight lower than 10%. When using urea and citric acid as organic fuels, the chemical reaction was not rigorous when compared with glycine and alanine. Moreover, the crystal structure and microstructure of Ni-Zn ferrites prepared by combustion technique with various organic fuels was studies also. They result show that the pure phase of Ni-Zn was obtained while using glycine, alanine and corbohydrazide. While using urea and citric as organic fuels, the impurities phase was obtained existed in the diffraction pattern, as seen in Figure 9. The nanocrystalline sizes are ranging between 20.2 and 43.7 nm, as seen in Table 2. The results indicated that the ceramic synthesized by the combustion technique produced nanocrystalline sizes.

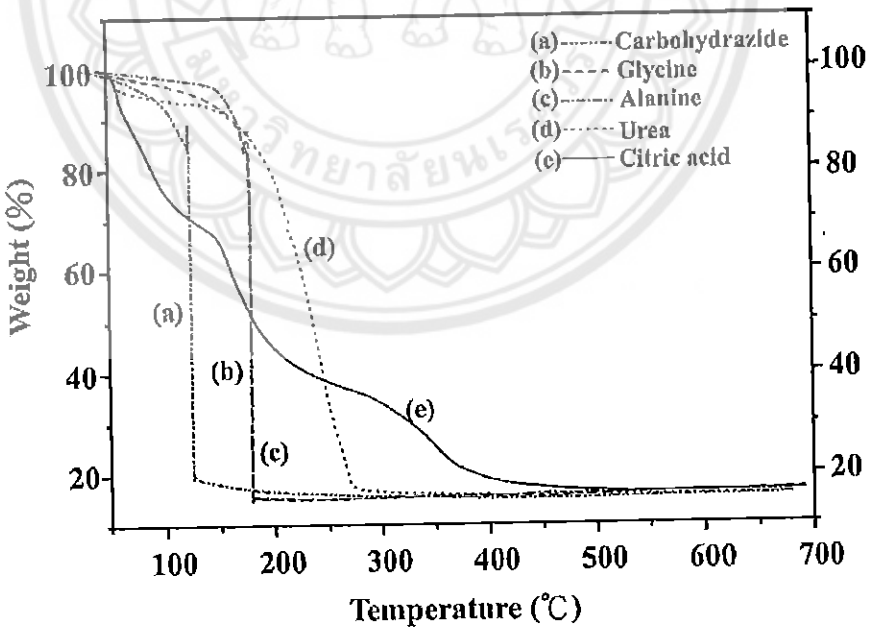

Figure 8 Thermogravimetric of various fuels [34]

Table 2 Oxide materials prepared by solution combustion method with the fuels

Material	Fuel	Particle size	Application
Al_2O_3	U	4 μm	Abrasive
Al_2O_3-ZrO_2	U	20-45 nm	Cutting tool
MAl_2O_4 (M=Mn and Zn)	AM+U/CH/ODH/GLY	15-28 nm	Catalytic support
$MgAl_2O_4$	U	13-20 nm	Structure material
CeO_2-ZrO_2	ODH	18 nm	Oxygen storage capacitor
	GLY	100 μm	Oxygen storage capacitor
$BaTiO_3$	GLY/CA	18-25 nm	Dielectric material
$Pb(Zr,Ti)O_3$	CA	~60 nm	Piezoelectric material
ZrO_2	GLY	23 nm	Oxygen sensor
$LiMn_2O_4$	PAA	30-60 nm	Lithium battery
$In_xGa_{1-x}O_3$	HY	54-160 nm	Optical coating for sensors
TiO_2	ODH	20 nm	Catalyst
	GLY	8-12 nm	Carcinogenic hexavalent chromium reduction
$LaBO_3$	U	55-75 nm (FESEM)	Decomposition of N_2O to N_2 and O_2
WO_3	GLY/U/thiourea	12-59 nm	Removal of organic dye from water
MgO	GLY	12-23 nm	Fluoride removal from drinking water

Note: U urea, AM metal acetate, CH carbohydrazides, ODH oxalidihidrazida, GLY glycine, CA citric acid, PAA poly acrylic acid, HY hydrazine. [35, 36, 37]

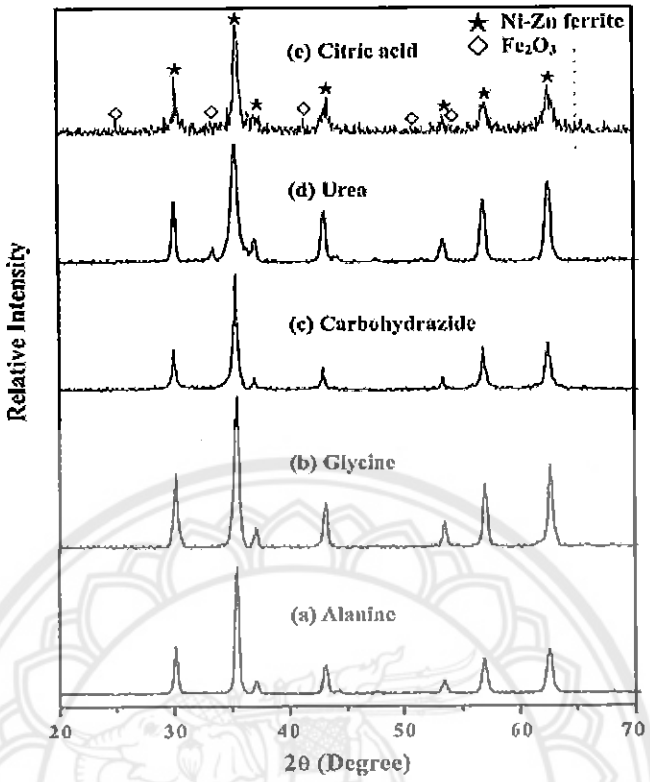

Figure 9 XRD patterns of the Ni-Zn ferrites with various organic fuels: (a) alanine (b) glycine (c) carbohydrazide (d) urea and (e) citric acid [34]

Wu, et al. [38] studied the effect of using various fuels on the structure and magnetic properties of SiO_2-doped Ni-Zn ferrite composite prepared by sol-gel combustion method. The result shows that the fuel type dramatically influenced the phase formation and electromagnetic properties of final products. The particle size for preparing its powders decreased in order: glycine route > hydrazine route > citric acid route, which are 34, 22 and 18 nm, respectively. Thus, citric acid was an effective chelating agent in producing fine ferrite powder. However, the glycine route was an effective fuel to possess the best magnetic properties with high saturation magnetization and low value of coercively.

Table 3 Effect of various fuels of the Ni-Zn ferrites prepared by the combustion technique [34]

Fuel	[a]T_m (°C)	Amount of gas produced (mole)	Crystallite size[b] (nm)	Surface area (m^2/g)	Carbon content (wt.%)	$Ni^{2+}:Zn^{2+}:Fe^{3+}$	M_s[c] (Am^2/kg)
Alanine	1245	20.7	38.6	24.7	1.64	0.500:0.467:1.920	60.8
Glycine	1150	26.2	32.7	31/2	1.53	0.500:0.471:1.922	62.4
Carbohydrazide	1380	24.0	43.7	20.6	1.87	0.500:0.462:1.917	58.5
Urea	785	30.7	20.2	48.5	3.82	0.500:0.483:1.936	57.2
Citric acid	725	26.2	22.7	44.1	5.75	0.500:0.490:1.947	55.8

Note: [a]T_m the maximum combustion temperature, measured by Pt-Pt-Rh thermocouple.

[b]Crystalline size of the as-synthesized Ni-Zn ferrite powders calculated from the line broadening of the (311) XRD peak by Sherrer formula.

[c]M_s the saturation magnetization of the sintered Ni-Zn ferrite samples (950 °C/2h).

Lead free piezoelectric ceramics

Many of the piezoelectric materials used today are lead-based. The PZT family mentioned initially is the most common one. This is the binary solid solution of $PbZrO_3$ an antiferroelectric (orthorhombic structure) and $PbTiO_3$ a ferroelectric structure (tetragonal perovskite structure). PZT has the perovskite structure with the Ti^{+4} and Zr^{+4} ions at B site at random. The phase diagram shows that at high temperature PZT has the cubic perovskite structure which is paraelectric and on cooling below the curie point the structure under goes a phase change from the ferroelectric tetragonal phase to rhombohedral phase. PZT dominates the field of

piezoelectrics because of its strong piezoelectric effect, especially at the compositions near the morphotropic phase boundary $Pb(Zr_{0.52}Ti_{0.48})O_3$, where two ferroelectric phases tetragonal and rhombohedral coexist at the room temperature. The morphotropic phase boundary of PZT is almost vertical in the phase diagram, as shown in Figure 10 which maintains the excellent piezoelectric properties across a wide temperature range [1].

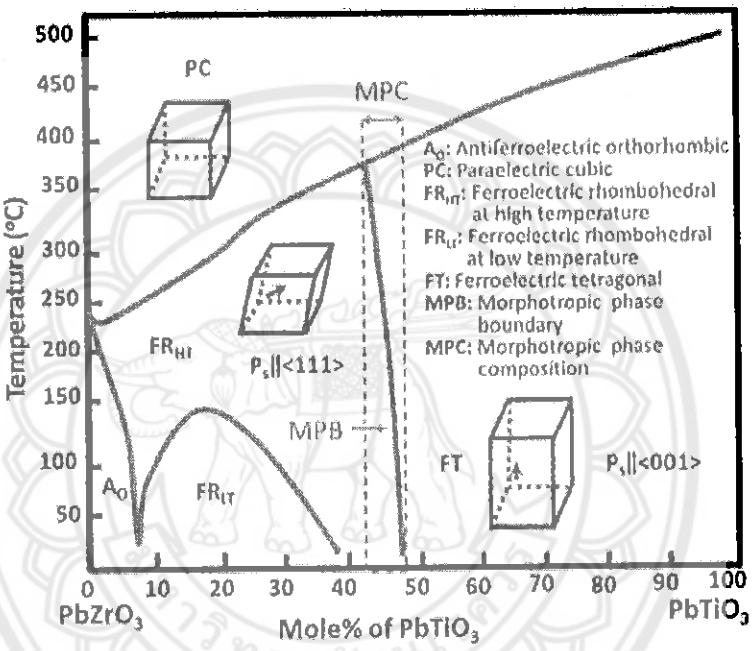

Figure 10 The phase diagram of PZT [1]

Some newer generations of lead-based piezoelectrics that exhibit exceptional piezoelectric properties have also been created by combining $PbTiO_3$(PT) with some lead-based ferroelectrics such as $Pb(Zn_{1/3}Nb_{2/3})O_3$ (PZN) and $Pb(Mg_{1/3}Nb_{2/3})O_3$ (PMN) to form solid solutions. Also, these materials show very high dielectric constants at room temperature owing to the broadening of the permittivity peak around the Curie temperature. PZT ceramics with MPB composition can also be doped with different ions and form "hard and soft" PZT is depending upon the requirements for certain applications [1].

The essential deficiency of Pb-based (PT, PZT and PMN) concerns its lead content. The amount of Pb in the usual Pb-based ceramics is more than 50 wt%, and once the Pb comes into the human body, it collects in various organs, leading potentially to serious effects to foetus, infertility, cancer and so forth. Note that not only the Pb in Pb-based compounds such as PT, PZT and PMN but also the PbO using as a raw material are known to dissolve when it is exposed to an aqueous environment However, high volatilization of PbO and its toxicity can pollute the environment and damage to human health, and then engender a terrible problem of environment pollution. However, these ceramics are toxic in the environment and damage to human health. The best way of prevention is to avoid the contact with leaded materials. Therefore, it is necessary in the search for lead-free piezoelectric materials to replace PZT ceramics.

Therefore, enormous efforts have been considerate in last decade for the development of competitive lead free counterparts, for example $BaZrO_3$ (BZ) based perovskite.

Barium zirconate

Barium zirconate ($BaZrO_3$) is one of the perovskite material with an ideal cubic structure and has a high melting point of about 2,600 °C. Barium zirconate is a good candidate for many applications.

A.M. Azad and S. Subramaniam [6] synthesized pure cubic perovskite $BaZrO_3$ powder using the solid reaction method and a sintered temperature from 1200 to 1700 °C. The x-ray diffraction patterns of $BaZrO_3$ ceramics were shown in Figure 11. All samples exhibited pure perovskite structure and no secondary phase could be found in all samples. The crystallite size ranged between 0.36 and 0.44 μm. The microstructural development in samples soaked for 6 h at 1400 and 1500 °C was shown in Figure 12. The microstructure reveals better intergranular connectivity, systematic grain growth and steadily diminishing porosity. However, the bodies sintered in the range 1200-1400°C were quite fragile and had a rather low strength. The sintered pellets could easily be broken under slight pressure. With increase in sintering temperature (1500–1700°C), densification improved systematically with corresponding decrease in porosity (mainly open pores). The average size is less than 1 μm in all the cases. the

compacts showed increase in strength, especially those sintered at 1600 and 1700 °C as shown in Figure 13.

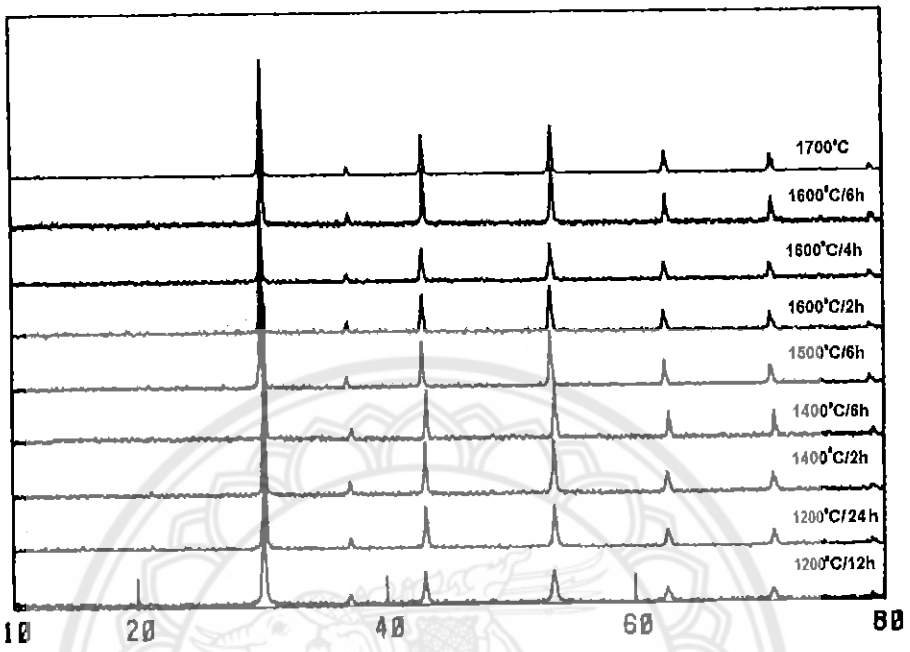

Figure 11 XRD patterns of $BaZrO_3$ sintered in the range 1200–1700 °C [6]

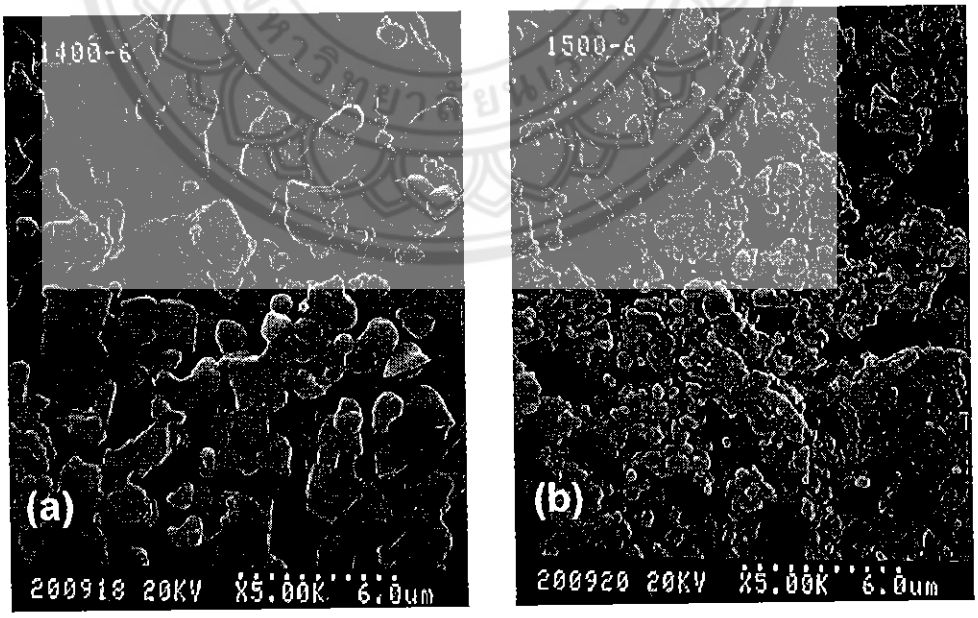

Figure 12 Microstructural development (clockwise) in $BaZrO_3$ soaked for 6 h at (a) 1400 and (b)1500 °C [6]

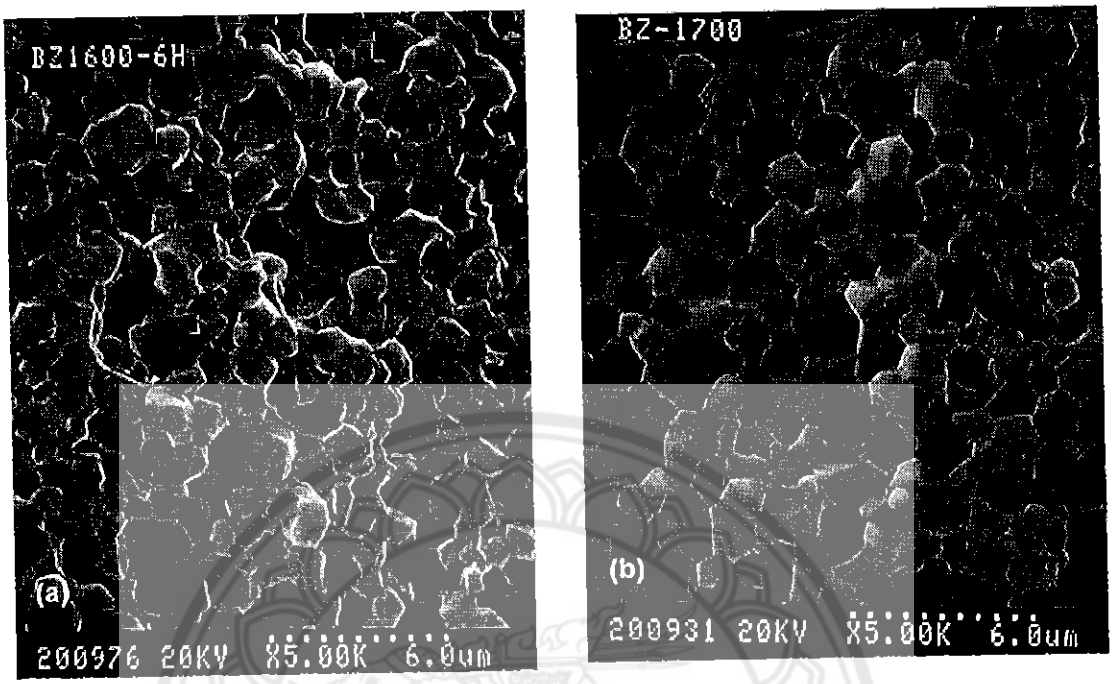

Figure 13 Enhanced densification and intergranular connectivity in $BaZrO_3$ sintered at (a) 1600°C and (b) 1600°C for 6h and 1700 °C no soak [6]

Sin, et al. [7] reported a value of 95% of theoretical density of $BaZrO_3$ ceramics. They synthesized nano $BaZrO_3$ powders by the polyacrylamide method. The sintered ceramics were obtained using a heat treatment of 1,500 °C for 10 h. Ganguli, et al. [18] synthesized Nano $BaZrO_3$, powders (25-30 nm) and low firing temperatures (calcined at 800 °C, sintered at 1,000 °C) were obtained using microemulsion route. Guillaume et al. [9] successfully prepared 99% of theoretical density of $BaZrO_3$ ceramics by control the calcined powder size distribution. The mean particles size of 600 nm was sintered at 1,650 °C for 2 h.

A.M. Azad and S. Subramaniam [10] attempted to improve the density and dielectric properties by adding 5 mol% Sn in $BaZrO_3$. The attempt to improve the density was not successful but with a dielectric loss of the $Ba(Zr_{0.95}Sn_{0.05})$ ceramics exhibited a very small value and were stable in a wide frequency range ($1\text{-}10^6$ Hz).

Li, et al. [11] studied the system of $(Ba_{1-x}Ca_x)(Ti_{0.94}Sn_{0.06})O_3$ (BCST) (x=0.01-0.04) ceramics by the solid state reaction technique. The microstructure of BCST ceramics at x = 0.01 is inhomogeneous and some pores exist in the grain boundary. For the samples at x = 0.02 and 0.03, the microstructure is homogeneous and no pore exists in the grain boundary, while the grain size is about 10 μm. For the sample at x = 0.04, the microstructure is inhomogeneous and the grain size becomes small (5 μm) as shown in Figure 14. The relative density are 96%, 98%, 99% and 97% for the BCST.

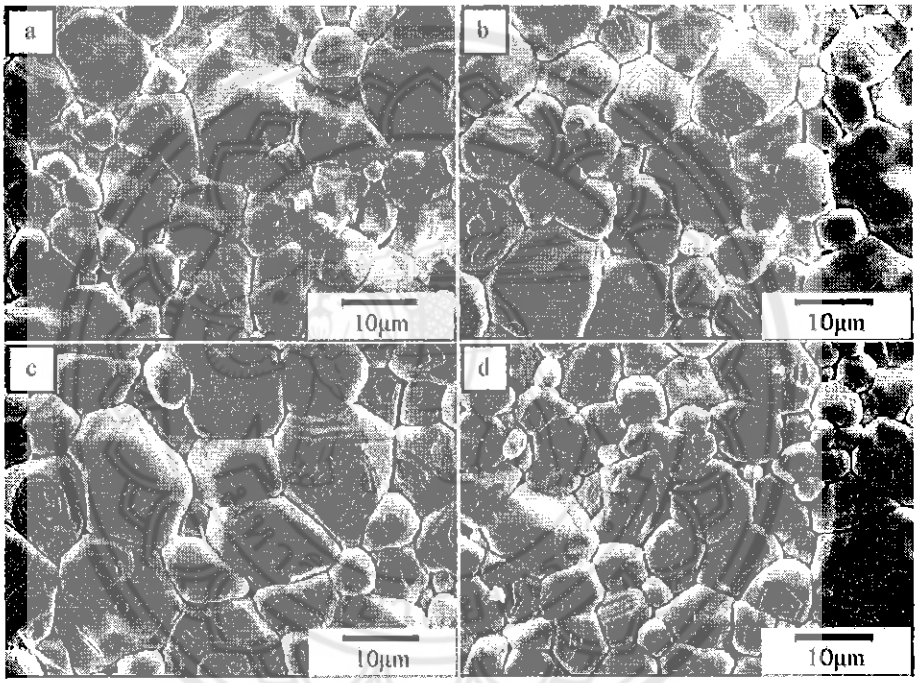

Figure 14 SEM micrographs of the $(Ba_{1-x}Ca_x)(Ti_{0.94}Sn_{0.06})O_3$ ceramics (a) x = 0.01, (b) x = 0.02, (c) x = 0.03 and (d) x = 0.04 [11]

The substitution of Ca promoted the microstructure of $Ba(Ti_{0.94}Sn_{0.06})O_3$, which presented a clear grain boundary and a uniformly distributed grain size. It also resulted in increased density and better electrical properties. $(Ba_{0.97}Ca_{0.03})(Ti_{0.94}Sn_{0.06})$ which exhibited excellent piezoelectric properties (d_{33}=440 pC/N, kp=45%), a high dielectric constant (ε_r= 6,900) and a low dielectric loss (tan δ=0.015).

CHAPTER III

MATERIALS AND METHOD

In this chapter explains the fabrication and characterization of BCZS. All powders fabrications were prepared by the solid state combustion method. The characterizations of these powders were observed using XRD, SEM and TEM. The ceramics were characterized to find out their properties such as physical properties, phase formation, microstructure and electrical properties. The details are presented in the following sections.

Powders Preparation

Fabrications of BCZS, including powders preparation fabrication have been described as follow:

Preparation of BCZS powder

Barium calcium zirconate stannate $(Ba_{0.97}Ca_{0.03})(Zr_{0.94}Sn_{0.06})O_3$: BCZS powder was synthesized using the combustion method. The starting raw materials were commercially available $BaCO_3$, $CaCO_3$, ZrO_2 and SnO_2, are listed in Table 4. The mixture of the raw materials were ground by a ball milling procedure (zirconia milling in an ethanol media for 24 h). Drying was carried out at 120°C for 4 h. The raw materials powders were well-mixed with the fuel (glycine) in the ratio of 1:2 by weight. The mixed powders were calcined at temperatures ranging from 1,000 to 1,200 °C with dwell time of 2 h and a heating/cooling rate of 5°C/min. The calcined powders were analyzed by X-ray diffraction technique to determine the amount of the perovskite phase percentage as shown in Figure 15.

Table 4 Specifications of starting materials used in preparation of BCZS powder

Materials	Source	Formula weight (g/mol)	Purity (%)
$BaCO_3$	Univar	197.34	99.00%
$CaCO_3$	Riedel-de Haën	100.09	98.50%
ZrO_2	CERAC	123.22	99.00%
SnO_2	Sigma-Aldrich	150.71	99.90%

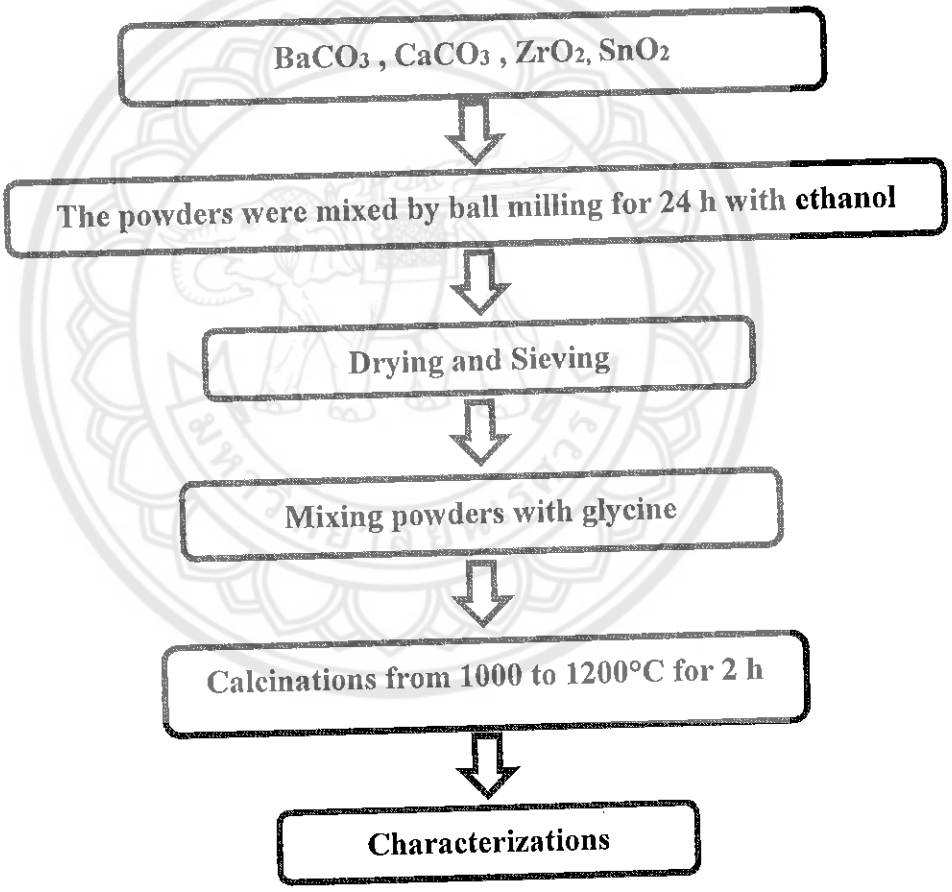

Figure 15 Schematic flow chart of BCZS powder preparation

Preparation of BCZS ceramics

After calcination, the calcined powders were mixed with 3 wt.% polyvinyl alcohol (PVA, Fluka) solution which was used as binder. They were then ball milled again for 24 h then the mixed solution was dried, crushed and sieved. The mixed calcined powders were pressed into disks with a diameter of 15 mm at a pressure of 80 MPa. Binder was burned out on sintering step at temperature 500 °C for 1 h. Afterwards, the green pellets of BCZS were sintered at various temperatures using a heating rate of 5°C/min and dwell time of 2 h. The flow chart of the BCZS ceramic fabrication is illustrated in Figure 16.

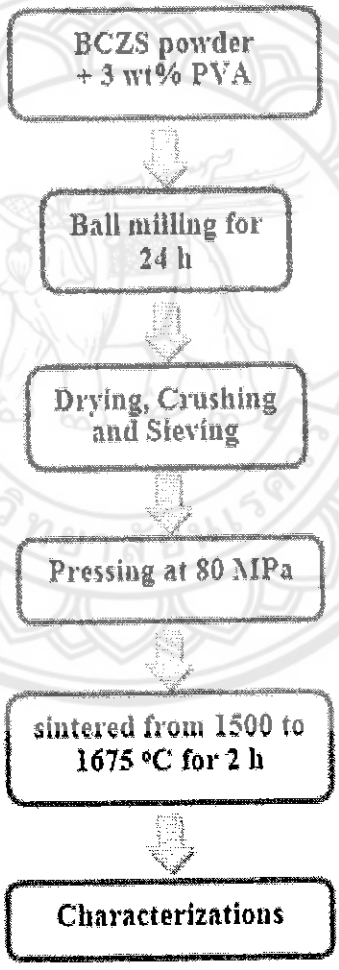

Figure 16 Schematic flow chart of BCZS ceramics preparation

Sample Characterization

The following section addresses the main characterization techniques used to investigate the phase formation, morphology, particle size, microstructure, physical properties and dielectric property of the samples in this study. They are described below.

X-ray diffraction (XRD) Technique

The X-ray diffraction (XRD) was used to identify the optimum firing temperatures, for phase identification, quantitative analysis of the mixtures of phases, and also to determine the crystal structure of the samples at room temperature, in both powder and ceramic forms. The X-ray diffractometer (Philips model X'Pert Pro) with Cu Kα radiation at 20 kV was employed as shown in Figure 17. Each sample was scanned for a 2θ range from 10°-60°. Lattice parameters of sample were determined from X-ray powder diffraction database from ICDD. The crystallite size of the calcined powder and ceramics grain size were also determined using the XRD line broadening as derived by Scherer equation [39];

$$B_{crystallites} = \frac{k\lambda}{L\cos\theta} \tag{5}$$

Where B is a broadening of the diffraction line measured at half its maximum intensity, L is the average crystallite size and k is a constant

The relative amounts of the perovskite and pyrochlore phases were calculated from the intensities of major X-ray reflections of the pyrochlore phase as perovskite phase using the equation proposed by Swart and Shrout [40];

$$\%Perovskite = \frac{I_{perovskite}}{I_{perovskite} + I_{pyrochlor}} \times 100 \tag{6}$$

Where $I_{perovskite}$ refers to the intensity of the peak of the perovskite phase and $I_{pyrochlore}$ refers to the intensity of the highest peak of pyrochlore phase.

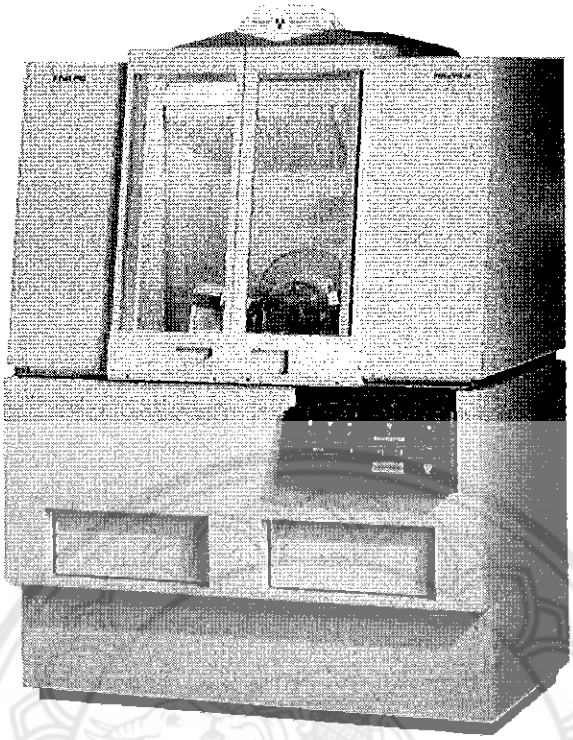

Figure 17 X-ray diffractometer [41]

Scanning electron microscopy (SEM)

Microstructural characterization of sample surface using scanning electron microscopy (SEM) (Figure 18) was performed to determine the grain size and the presence of porosity. Average grain size of the sintered ceramics were estimated by using a linear intercepting method, where random linear lines (L) were drawn on each SEM micrograph and the number of the intercepts which the grain boundary makes with the line (N). The average grain size (D) was determined from measurements along random lines using the equation [52];

$$D = \frac{L}{N} \tag{7}$$

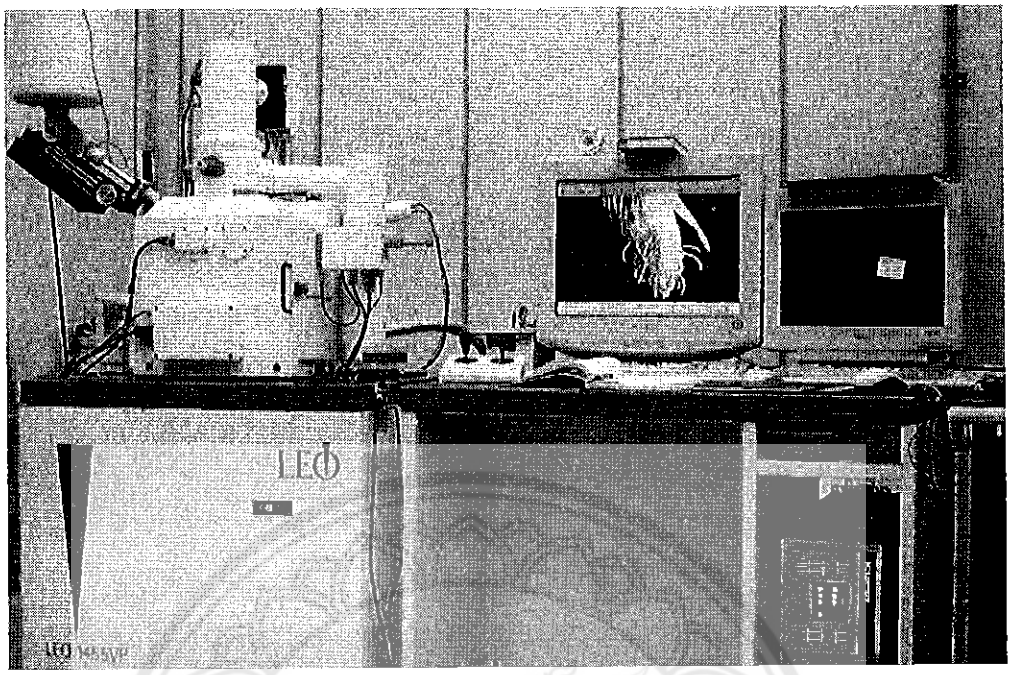

Figure 18 Scanning electron microscopy [41]

Transmission electron microscopy (TEM)

Transmission electron microscopy (TEM) (Figure 19) was employed to investigate the morphology of the powders. Samples for TEM were prepared by grinding, dispersing them in isopropyl alcohol and then depositing the sample by pipette onto 3 mm holey copper grids for observation by TEM (FEI, Technai G2).

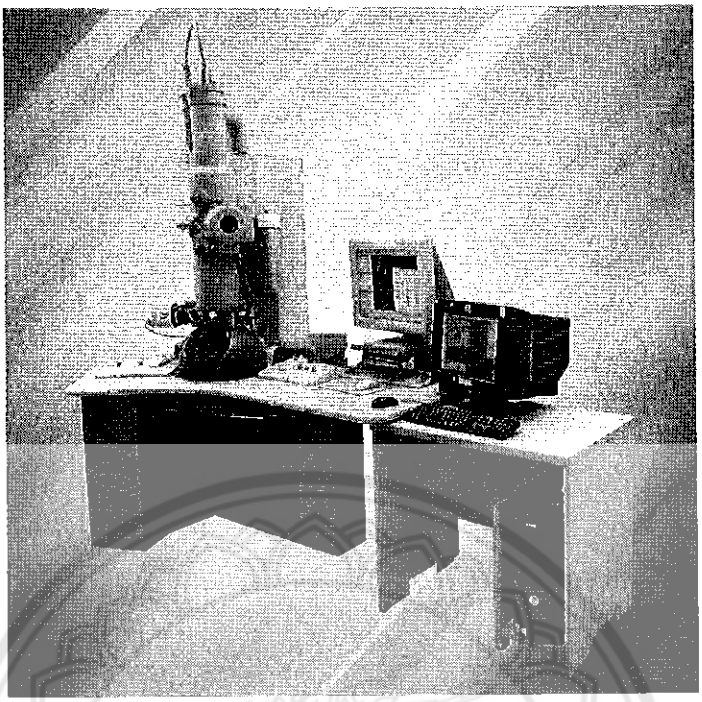

Figure 19 Transmission electron microscopy [41]

Densification analysis

The method of measuring the density of a piece of ceramics material usually described in standards is based on the Archimedes principle. This principle stated the weight of an object in a fluid equals it's by weight minus the buoyant force (or the weight of the fluid displaced). However, it is usual to measure open porosity levels at the same time by ensuring that during immersion liquid can penetrate all parts of the specimen through the open porosity. Typical procedures are;

1. Dry specimen(s) in air at 110 °C, store in a desiccator, weigh when cold (mass W_1)

2. Boil in distilled water for a period, typically 3 hours and leave it for 1 night

3. Weigh immersed in water (W_2) and then weight during immersion liquid can penetrate all parts of the specimen through the open porosity (W_3).

4. Calculate follow this equation:

$$\rho_c = \frac{W_1 \rho_w}{W_3 - W_2} \tag{8}$$

where, ρ_w is the density of water at room temperature (g/cm^3) and is the density of sample at room temperature (g/cm^3); however the density of water is slightly temperature dependent

$$\rho_w = 1.0017 - 0.0002315T \quad (9)$$

Moreover, the fired shrinkage of all sintered ceramics were measured from the percentage diameter change with respect to the original diameter (l_0) before sintering;

$$Shrinkage(\%) = (\frac{l_1 - l_0}{l_0})x100 \quad (10)$$

where l_1 is diameter of pellet before sintering (mm),
l_0 is diameter of pellet after sintering (mm)

Dielectric measurement

The dielectric properties of the sintered ceramics were studied as functions of both temperature and frequency with an automated dielectric measurement system. The measurement system which measured the dielectric properties consisted of a LCR meter (Agilent 4263B). The dielectric properties were determined over a temperature range from room temperature to 200 °C with different frequencies (3 frequency of 1 kHz, 10 kHz and 100 kHz). The dielectric constant (ε_r) was calculated with the following equation,

$$\varepsilon_r = \frac{Cd}{\varepsilon_0 A} \quad (11)$$

where ε_0 is the permittivity of free space,
C is the capacitance,
D is the thickness of the sample,
A is the area of the sample.

P-E measurement

P-E measurement was made using high voltage amplifier (Trek), precision High Voltage Interface (HVI, Radiant Technologies), precision LC (Radiant Technologies) and computerized control and data acquisition. The sample is placed in a High Voltage Test Fixture chamber (HVTF) chamber in bottom half of the fixture. A copper electrode fixed in the bottom of the chamber contacts the electrode on the bottom of the sample. The bottom chamber is sealed so it may be filled with insulating oil to protect the sample from the arcing that may occur in open air. The system is an automated device intended for measuring the polarization of materials induced by a single triangle wave. It can prevent the excess voltage and current during a sample breakdown from exceeding the current canceling capability of the virtual ground circuitry on the tester input. During the measurement, an electric field of 30 kV/cm based on the coercive field was applied to a sample which immersed in a silicone oil to prevent the breakdown of the sample.

Piezoelectric properties measurement

The optimum poling conditions were determined by poling the KNLNTS ceramics with applying DC field of 3 kV/mm in a stirred oil bath at 80°C for a time period 30 minutes. The piezoelectric constant (d_{33}) was measured using a quasi-static piezoelectric d_{33} meter. The piezoelectric constant (d_{33}) measurements were made directly after poling and after 24 hours. Measurements were conducted at a drive frequency of 100 Hz.

CHAPTER IV

FABRICATION OF NEW $(Ba_{0.97}Ca_{0.03})(Zr_{0.94}Sn_{0.06})O_3$ CERAMICS BY THE SOLID STATE COMBUSTION TECHNIQUE

In this chapter, the results are presented for the investigation of $(Ba_{0.97}Ca_{0.03})(Zr_{0.94}Sn_{0.06})O_3$ (BCZS) ceramics using solid state combustion technique. There are effects of calcination temperature and sintering temperature on crystal structure, microstructure and dielectric properties of BCZS ceramics. The details of results are presented as followed.

Results and Discussion

The X-ray diffraction patterns of the calcined BCZS powders between 1,000 and 1,200 °C for 2 h are shown in Figure 20. The diffraction lines were indexed on the basis of a cubic structure. A trace amount of ZrO_2 secondary phase (according to JCPDS file number 05-0543) was found below 1,150 °C. The pure perovskite phase was found at higher than 1,150 °C which could be matched with the JCPDS file number 06-0399. The percentage of the BCZS perovskite phase increased with an increase of calcination temperatures as seen in Table 5.

Table 5 Percent perovskite phase and average particle size of BCZS powders

Calcined temperature (°C)	Percent perovskite phase	Average particle size [FWHM] (nm)
1,000	93.6	73
1,050	95.9	79
1,100	99.3	93
1,150	100	98
1,200	100	103

The crystalline size of the BCZS powders calculated from Full Width at Half Maximum (FWHM) using the Scherrer's equation. The average particle sizes tended to increase from 73 to 103 nm as calcination temperatures increased.

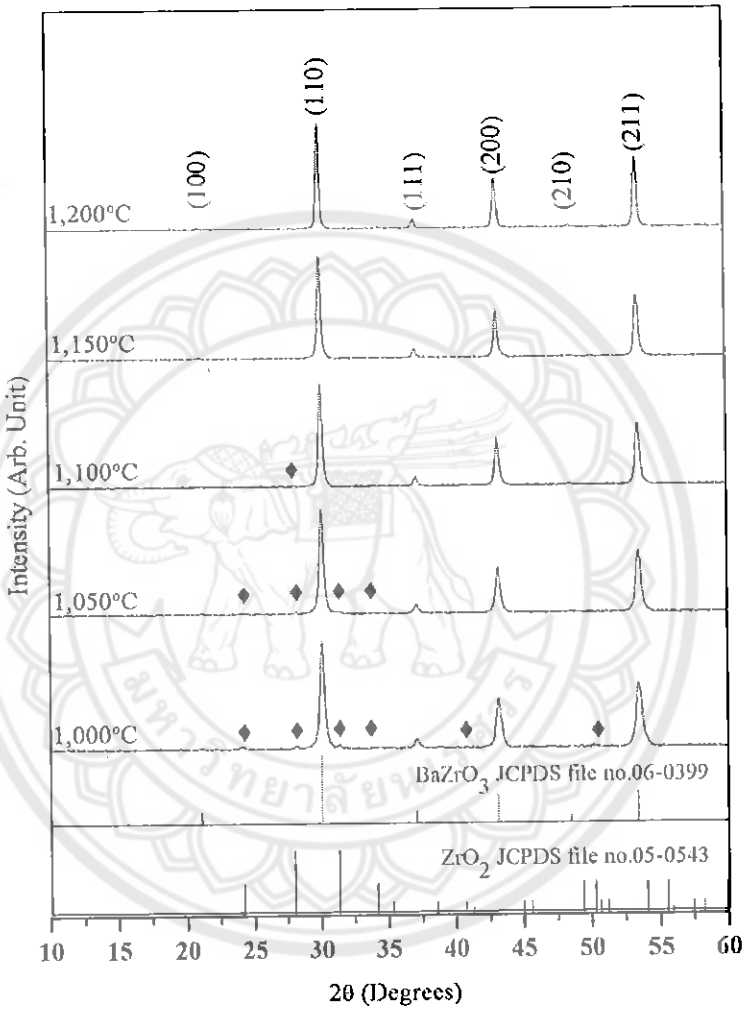

Figure 20 XRD patterns of BCZS powders calcined at various temperatures for 2 h; (♦) ZrO_2

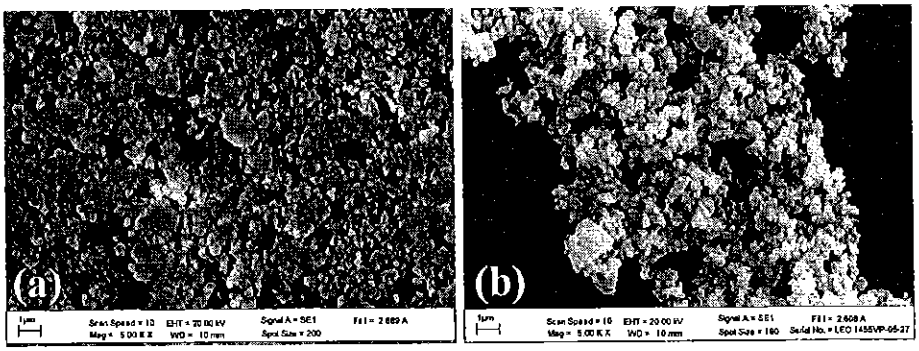

Figure 21 SEM photographs of BCZS powders calcined at (a) 1,000°C and (b) 1,200°C

The SEM photographs of BCZS powders calcined at difference temperatures are shown in Figure 21 (a) and (b). The BCZS calcined powders exhibited a rather spherical shape. The BCZS particles, observed in the sample calcined at 1000°C for 2 h (Figure 21 (a)), were tightly agglomerated. The agglomerates demonstrated a wide size distribution and an irregular shape. At higher calcined temperatures, loosely bound agglomerates with a narrow distribution were observed (Figure 21 (b)). Generally, Pure $BaZrO_3$ powders can easily form the agglomerate characteristics. Moreover, highly dense and large agglomerate (20 μm) powders are formed at high calcined temperature [16]. For this result, it was found that the replacement of Ca and Sn in the A-site and B-site of $BaZrO_3$ powders can reduced the agglomeration size of the calcined powders (~2 μm) and it was decreased by higher calcination temperature.

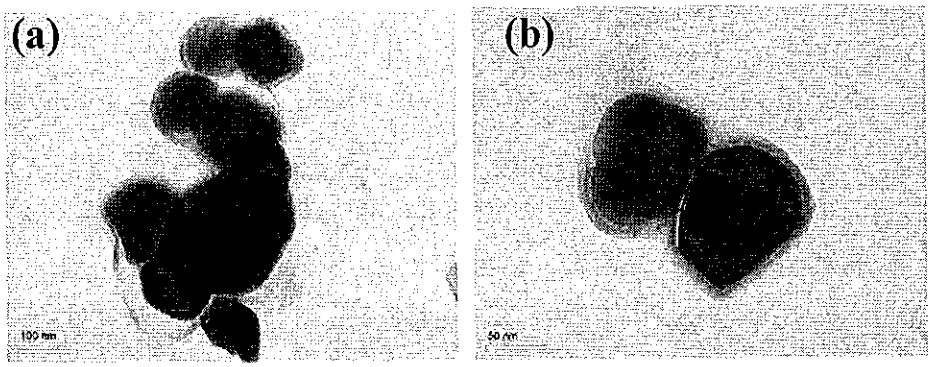

Figure 22 TEM micrograph of BCZS nanopowders calcined at 1,150°C (a) low magnification image and (b) high magnification image

Figure 22 shows typical TEM micrographs of pure BCZS powders calcined at 1150°C for 2 h. The powders exhibited agglomerate particles and wide agglomerate size which consisted of rather spherical shaped particles when observed by TEM in a low magnification image as shown in Figure 22 (a). It was observed that an the opaque area appeared at the centre and edge of some segments. This was caused from particles massively agglomerate which an electron can not be transmitted. The gauzy region was observed as a small segment in which electrons were able to transmit through but an accurate particle size could not be obtained. A definite particle size was observed by using very high magnification (Figure 22 (b)). It was found that many fine particles with a particle size around 96 nm existed. The particle size was close to the particle sizes calculated by FWHM. This confirmed that the combustion technique was capable or producing pure BCZS nanopowders. This is crucial for the production of dense ceramic bodies with high strength.

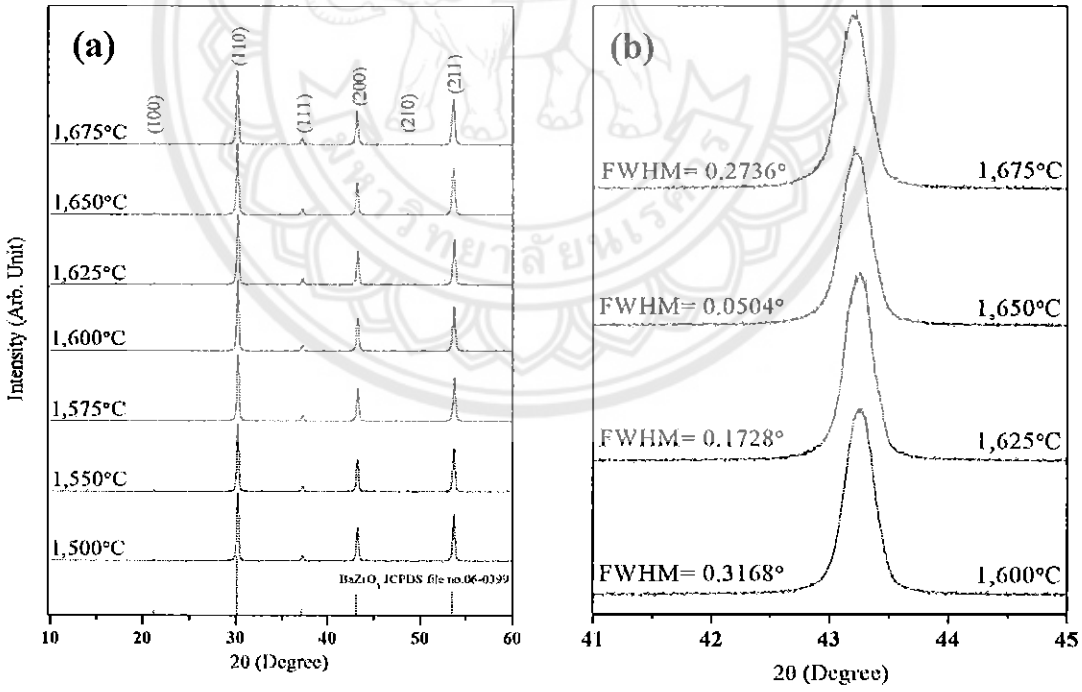

Figure 23 XRD patterns of BCZS ceramics (a) at 2θ between 10° and 60° (b) at a very low scanning rate of 2θ between 41° and 45°

The pure BCZS nanopowders calcined at 1,150 °C were pressed into pellets and sintered from 1,500-1,675 °C for 2 h. Figure 23 (a) shows the XRD patterns in the 2θ range from 10° to 60° of the BCZS ceramics at different sintering temperatures. All samples were free from secondary phase. BCZS ceramics were identified as having a single phase with a cubic perovskite structure which matched with the JCPDS file number 06-0399. The lattice parameter *a* of the BCZS sintered ceramics was calculated and is listed in Table 6. The lattice parameter *a* increased with the increase of sintering temperatures. The XRD patterns measured from 41 to 45 ° at a very low scanning rate (step size 0.002897°, time/θ 7.44 s, scan speed 0.012075°/s) and are shown in Figure 23 (b). It can be seen that the diffraction angle decreased with increasing sintering temperatures. The diffraction peak exhibited a sharper curve when increasing the sintering temperature up to 1,650 °C. The FWHM of 1675°C sintered ceramic was wider than 1,650 °C sintered sample. This indicated at a lower sintering temperature of 1,650 °C, the crystallinity is increased with an increase of sintering temperature.

Table 6 The lattice parameter *a*, average grain size, linear shrinkage and density of BCZS ceramics

Sintered temperature (°C)	Lattice parameter *a* (Å)	Average grain size (μm)	Linear shrinkage (%)	Measured density (g/cm^3)
1,500	4.1744	0.51	10.45	4.86
1,550	4.1750	0.74	12.57	5.14
1,575	4.1765	0.97	12.97	5.22
1,600	4.1777	1.53	13.03	5.57
1,625	4.1789	1.54	14.69	5.67
1,650	4.1816	1.58	14.95	5.86
1,675	4.1874	1.61	-	-

Figure 24 (a)-(f) show the SEM photographs of the surface of the BCZS ceramics sintered between 1,500 and 1,675 °C. At a sintering temperature of 1500 °C, the intergranular connectivity with a loose bond, high porosity and small grain were observed (Figure 24 (a)). With higher sintering temperatures, the grain rapidly grew and was highly connected intergranularly (Figure 24 (b) and (c)). By increasing the sintering temperature, the pore structure continuously reduced (Figure 24 (b) and (c)). When increasing the sintering temperature, grains grew continuously and the surface characteristic was changed from unfulfilled to complete morphology (Figure 24 (d)-(f)). The minimizing of pore structure and a more uniform distribution of grain size occurred when sintering temperatures increased from 1,625 to 1,650 °C (Figure 24 (d) and (e)). In Figure 24 (f), the grain boundary of the BCZS ceramics stared to melt and then it was unclearly observed for the sample sintered at 1,675 °C. The microstructural result corresponded to the XRD result. The average grain size increased from 0.51 to 1.61 μm with increasing sintering temperature as listed in Table 6.

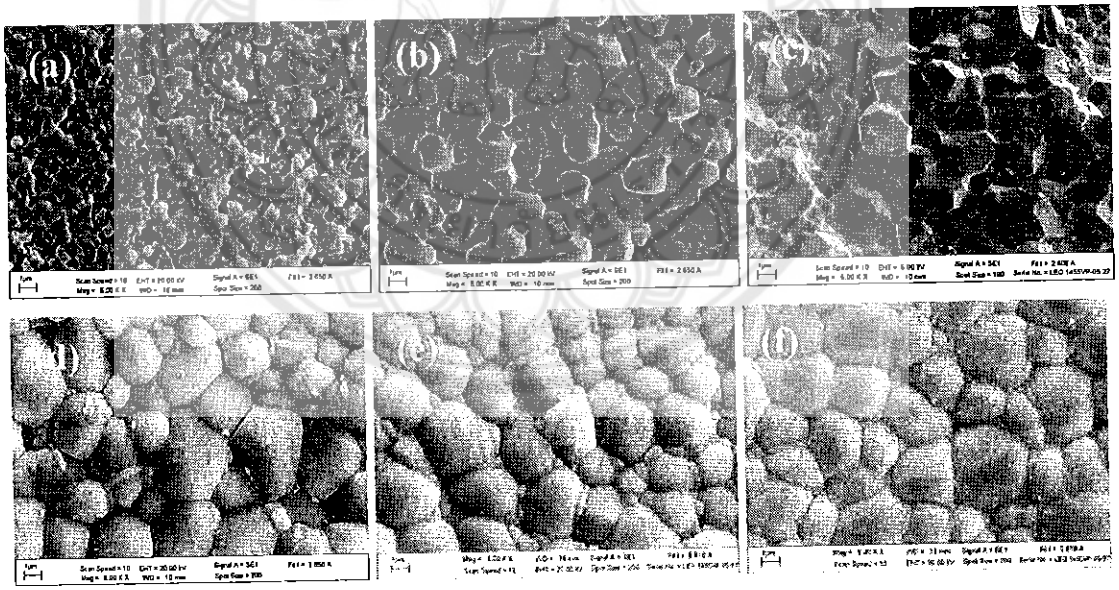

Figure 24 SEM photomicrographs of the BCZS ceramics sintered at (a) 1,500°C, (b) 1,575°C, (c) 1,600°C, (d) 1,625 °C, (e) 1,650 and (f) 1,675 for 2 h

The linear shrinkage and measured density at room temperature with a variation of the sintering temperatures are shown in Table 6. The percentage of shrinkage and density of the BCZS ceramics increased when sintering temperature increased. The maximum density (5.86 g/cm^3) was obtained by the sample sintered at 1,650 °C. The shrinkage and density of the pellets sintered at 1,675 °C could not be reported because of its fragility. The density result corresponded to the microstructure in the SEM results.

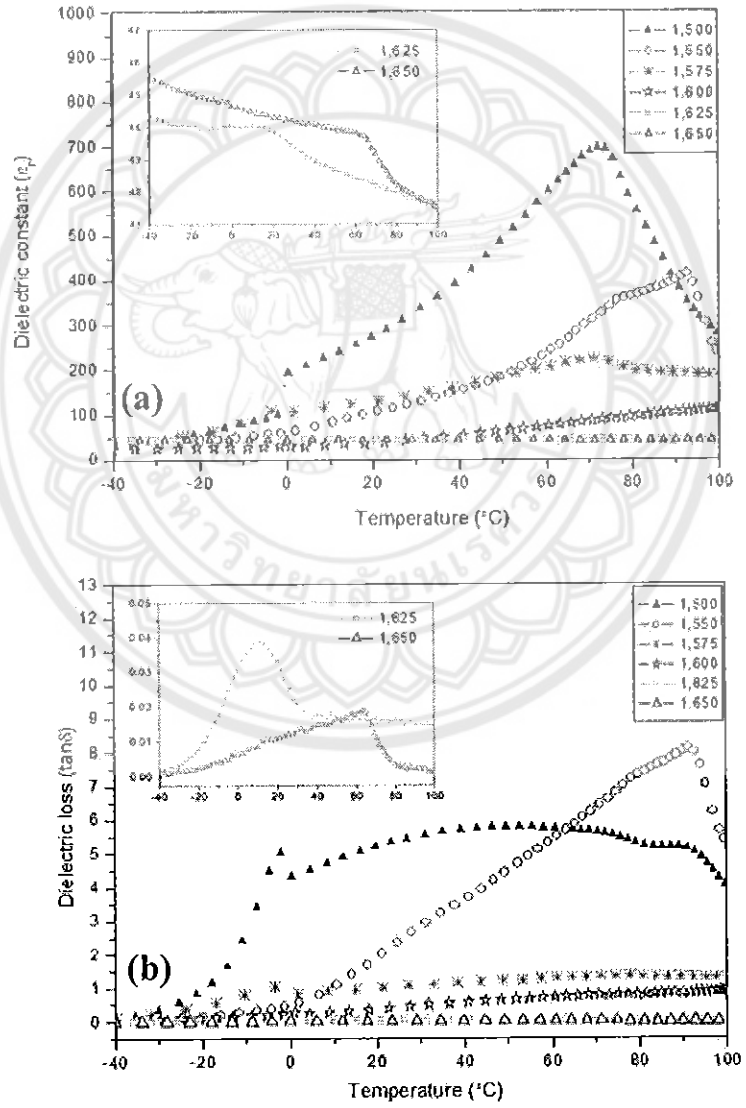

Figure 25 Temperature dependences of (a) dielectric constant and (b) loss tangent of the BCZS ceramics measured at 100 kHz

The temperature dependences of the dielectric constant (ε_r) and the dielectric loss (tan δ) of the BCZS ceramics sintered at various temperature and measured at the frequency of 100 kHz are shown in Figure 25. At low sintering temperatures between 1,500 and 1,575 °C, the ε_r and tan δ were not stable with increasing temperature and a high dielectric constant and high dielectric loss were observed. For the ceramics sintered at 1,600 °C, the ε_r and tan δ were reduced and more stable than those observed in low sintering temperature samples. At high sintering temperatures between 1,625 and 1,650 °C, the ε_r was nearly stable (42-45) with increasing temperature (inset Figure 25 (a)). The dielectric loss of the sample sintered at 1,650°C was lower than the sample sintered at 1,625°C (inset Figure 25 (b)). These results corresponded with the XRD, SEM and density results. The ε_r and tan δ values at room temperature of 1,650 °C of the sintered samples were 44 and 0.01, respectively. Ganguli, et al. [18] reported ε_r and tan δ (measured at 100 kHz) of $BaZrO_3$ prepared via the microemulsion route are 18 and 0.3, respectively. This indicated that the addition of Ca and Sn in $BaZrO_3$ prepared using the combustion technique can reduce the tan δ.

CHAPTER VII

CONCLUSION

A pure nano powders of $(Ba_{0.97}Ca_{0.03})(Zr_{0.94}Sn_{0.06})O_3$ (BCZS) were obtained at low a calcination temperature of 1,150 °C for 2 h using the combustion method. The firing temperatures strongly effected phase formation, microstructure, density and dielectric properties. The sample sintered at 1,650 °C exhibited the highest density, a stable dielectric constant and the lowest dielectric loss. The results of XRD, SEM, density and dielectric properties support each other.

In conclusion, the solid state combustion technique was successfully obtained to synthesize the BCZS nanocrystalline powders and ceramics. This study can be produce ultrafine BCZS powders uses a lower calcination temperature and leads to obtaining dense BCZS ceramics with good electrical properties.

REFERENCES

[1] Jaffe, B., Cook, W.R. and Jaffe, H. (1971). **Piezoelectric ceramics**. India: Ceramic Book and Literature Service.

[2] Maeder, M.D., Damjanovic, D. and Setter, N. (2004). Lead free piezoelectric materials. **Journal of Electroceramics,** 13, 385-392.

[3] Anselmi-Tamburini, U., Buscaglia, M.T., Viviani, M., Bassoli, M., Bottino, C., Buscaglia, V., et al. (2006). Solid-state synthesis and spark plasma sintering of submicron $BaY_xZr_{1-x}O_{3-x/2}$ (x=0, 0.08 and 0.16) ceramics. **Journal of European Ceramics Societies,** 26, 2313-2318.

[4] Erb, A., Walker, E. and Flukiger, R. (1995). $BaZrO_3$: The solution for the crucible corrosion problem during the single crystal growth of high-T_c superconductors $REBa_2Cu_3O_{7-\delta}$; RE=Y, Pr. **Physica C,** 245, 245-251.

[5] Kamitani, A., Wakana, H., Dachi, S. and Tanabe, K. (2004). Investigation of $BaZrO_3$ and $SrZrO_3$ insulating layers on La-YBCO ground plane for high-T_c devices. **Physica C,** 412-414, 1414-1418.

[6] Azad, A.M., Subrmaniam, S. and Dung, T.W. (2002). On the development of high density barium metazirconate ($BaZrO_3$) ceramics. **Journal of American Ceramics Society,** 334, 118-130.

[7] Sin, A., Montaser, B. El., Odier, P. and Weiss, F. (2002). Synthesis and sintering of large batches of barium zirconate nanopowders. **Journal of American Ceramics Society,** 85, 1928-1932.

[8] Ganguli, A.K., Ahmad, T., Vaidya, S. and Ahmed, J. (2008). Microemulsion Route to the synthesis of nanoparticles. **Pure and Applied Chemistry,** 80, 2451-2477.

[9] Guillaume, B., Boschini, F., Garcia-Cano, I., Rulmont, A., Cloots, R. and Ausloos, M. (2005). Optimization of $BaZrO_3$ sintering by control of the Initial powder size distribution; a factorial design statistical analysis. **Journal of American Ceramics Society,** 25, 3593-3604.

[10] Azad, A.M. and Subramaniam, S. (2002). Temperature dependence of the dielectric response of $BaZrO_3$ by immittance spectroscopy. **Materials Research Bulletin,** 37, 11-21.

[11] Li, W., Xu, Z., Chu, R., Fu, P. and Zang, G. (2012). Enhanced ferroelectric properties in $(Ba_{1-x}Ca_x)(Ti_{0.94}Sn_{0.06})O_3$ lead-free ceramics. **Journal of European Ceramics Societies,** 32, 517-520.

[12] Kornphom, C., Paowsawat, S. and Bongkarn, T. (2014). Phase formation, Microstructure and electrical properties of KNN-BZT ceramics fabricated via combustion technique. **Ferroelectics,** 458, 127-135.

[13] Bhupaijit, P., Kornphom, C., Vittayakorn, N. and Bongkarn, T. (2015) Structural, microstructure and electrical properties of La_2O_3-doped $Bi_{0.5}(Na_{0.68}K_{0.22}Li_{0.1})_{0.5}TiO_3$ lead-free piezoelectric ceramics synthesized by the combustion technique. **Ceramics International,** 41, S81-86.

[14] Yotthuan, S., Kornphom, C. and Bongkarn, T. (2015). The effect of firing conditions on phase formation, microstructure and dielectric properties of BNKTNb-LSb ceramics prepared via the combustion technique. **Phase Transitions,** 88, 1035-1043.

[15] Thawong, P., Kornphom, C., Chootin, S. and Bongkarn, T. (2016). Phase evolution and electrical properties of a new system of (1-x)[BNT-BKT-KNN]-xBCTZ lead-free piezoelectric ceramics synthesized by the solid-state combustion technique. **Phase Transitions,** 89, 232-241.

[16] Hench, L.L. and West, J. (1990). **Principles of Electronic Ceramics Hoboken**. New Jersey: John Wiley & Sons Incorporated.

[17] Haertling, H. (1999). Ferroelectric ceramics: History and Technology. **Journal American Ceramic Societies,** 82, 797.

[18] Moulson, A.J. and Herbert, J.M. (2003). **Electroceramics**. New York: Wiley- Interscience.

[19] Fousek, J. (1995). Joseph Valasek and the Discovery of Ferroelectricity. **Proceeding of the IEEE,** 1.

[20] Sawyer, C. B. and Tower, C. H. (1930). Rochelle Salt as a Dielectric. **Physics Review,** 35, 269.

[21] Jona F. and Shirane, G. (1962). **Ferroelectric crystal.** New York: Pergamum Press.

[22] Megaw, H. (1957). **Ferroelectricity in crystals.** London: Methuen.

[23] Chiang, Y. (1997). **Physical ceramics.** New York: John Wiley & Sons.

[24] Guo, R. (2000). Origin of the high piezoelectric response in $PbZr_{1/x}$ TiO_3. **Physics Review Letters**, 84, 5423.

[25] Ganguli, D. and Chatterjee, M. (1997). **Ceramic powder preparation**. USA: Kluwer Academic Publishers.

[26] Cahu, R.W., Haasen, P. and Kramer, E.J. (1996). **Materials sciences and technology**. Germany: The Federal Republic of Germany.

[27] Pierre, A.C. (1998). **Introduction to so-gel processing**. USA: Kluwer Acadamic Publishers.

[28] Ring, T.A. (1996). **Fundamentals of ceramics powder processing and synthesis**. New York: Acdemic Press Inc.

[29] Merzhanov, A.G. (1996). Combustion processes that synthesize materials. **Journal of Materials Processing Technology**, 56(1-4), 222-241.

[30] Pampuch, R. (1999). Advanced HT ceramic materials via solid combustion. **Journal of the European Ceramic Society**, 19(13-14), 2395-2404.

[31] Patil, K.C., Aruna, S.T. and Mimani, T. (2002). Combustion synthesis: An update. **Current Opinion in Solid State and Materials Science**, 6(6), 507-512.

[32] Chandradass, J., Balasubramanian, M., Bae, D.S. and Kim, K.H. (2009). Effect of different fuels on the alumina–ceria composite powders synthesized by sol–gel auto combustion method. **Journal of Alloys and Compounds**, 479(1-2), 363-367.

[33] Kopp Alves, A., Bergmann, C.P. and Berutti, F.A. (2013). **Novel synthesis and characterization of nanostructured materials**. N.P.: Springer Berlin Heidelberg.

[34] Hwang, C.C., Wu, T.Y., Wan, J. and Tsai, J.S. (2004). Development of a novel combustion synthesis method for synthesizing of ceramic oxide powders. **Materials Science and Engineering: B,** 111(1), 49-56.

[35] Patil, K.C., Aruna, S.T. and Mimani, T. (2002). Combustion synthesis: An update. **Current Opinion in Solid State and Materials Science**, 6(6), 507-512.

[36] Patil, K.C., Aruna, S.T. and Ekambaram, S. (1997). Combustion synthesis. **Solid State & Materials Science**, 2, 156-165.

[37] Aruna, S.T. and Mukasyan, A.S. (2008). Combustion synthesis and nanomaterials. **Current Opinion in Solid State and Materials Science,** 12(3-4), 44-50.

[38] Wu, K.H., Ting, T.H., Li, M.C. and Ho, W.D. (2006). Sol-gel auto-combustion synthesis of SiO_2-doped NiZn ferrite by using various fuels. **Journal of Magnetism and Magnetic Materials,** 298(1), 25-32.

[39] Suranarayana, C. and Grant Norton, M. (1998). **X-ray diffraction a practical approach**. New York: Plenum.

[40] Swartz, S.L. and Shrout, T.R. (1982). Fabrication of perovskite lead magnesium niobate. **Materials Research Bulletin,** 17(10), 1245-1250.

[41] **Science Lab Center**. (2004). Retrieved February 1, 2014, from http://www.sci.nu.ac.th/slcs/index.php.